Dihedral Effect of a Flexible Wing

WILLIAM P. RODDEN*
Aerospace Corporation, El Segundo, Calif.

The dihedral effect of a flexible wing is considered as a critical aeroelastic problem because of the importance of dihedral in determining lateral-directional dynamic stability and the large changes in dihedral that result from symmetrical wing bending during longitudinal maneuvers that approach limit load factor. Some recently declassified experimental data of the rolling moment caused by sideslip measured at low speed on an aeroelastic model of the Douglas XA3D-1 airplane are presented. A review of some early simplified methods of analysis is made, and the correlation of one of the methods with the experimental results is shown. Finally, the problem of estimating wing dihedral effect is reformulated in terms of structural and aerodynamic influence coefficients in order to utilize recent advances in lifting surface theory. The experimental data and other examples cited indicate that the aeroelastic change in dihedral effect at limit load factor can equal the value measured on rigid models.

Nomenclature

A = element of aeroelastic amplification matrix
A_s = element of static pressure-downwash influence coefficient matrix
$AICs$ = matrix of aerodynamic influence coefficients
a = element of structural influence coefficient matrix
B = element of pressure integration matrix
b = total wing span
C_{hs} = element of $AICs$ for symmetrical loading
$C_{h\beta}$ = element of $AICs$ for sideslipping
C_{l_p} = damping-in-roll coefficient
C_{l_s} = rolling moment coefficient about stability axis
C_{l_β} = dihedral effect, i.e., rolling moment coefficient due to unit sideslip angle
$(C_{l_\beta})_0$ = rigid vehicle dihedral effect
ΔC_{l_β} = aeroelastic increment in dihedral effect
$(\Delta C_{l_\beta})_\Gamma$ = aeroelastic increment caused by amplification of geometric dihedral
$(\Delta C_l)_n$ = aeroelastic increment caused by symmetrical load factor
$\bar{c}$ = mean aerodynamic chord
D_x = element of differentiation matrix in chordwise direction
D_y = element of differentiation matrix in spanwise direction
E = Young's modulus of elasticity
F = control point force
g = acceleration of gravity
h = deflection
h_t = deflection at wing tip
I = element of unit matrix
k = flexibility constant relating wing lift to tip deflection
L_w = wing lift
$\mathfrak{L}$ = rolling moment about stability axis
M = element of mass matrix
m = exponent in polynomial approximation to wing deflection curve
n = airplane symmetrical load factor
n_L = design limit load factor
q = dynamic pressure
S = area of *one* wing
t_r = airfoil thickness at wing root
V = airplane forward velocity
W = airplane gross weight; element of downwash differentiation matrix
w = downwash velocity
y = spanwise coordinate
α = angle of attack
α_g = geometric angle of attack in wind tunnel
α_0 = local downwash angle induced by geometric twist and camber
β = sideslip angle
Γ = geometric dihedral angle
η = dimensionless spanwise coordinate, $\eta = 2y/b$
λ = wing planform taper ratio
σ = design working yield stress for wing bending
ψ = yaw angle, $\psi = -\beta$

Subscripts and Matrix Notation

l = left wing
r = right wing
$[\ ]$ = square matrix
$\lceil\ \rceil$ = diagonal matrix
$[\ ]^{-1}$ = inverse matrix
$\{\ \}$ = column matrix
$[\ ]$ = row matrix

Received August 3, 1964; revision received January 6, 1965. The author wishes to thank the Douglas Aircraft Company, Inc. and Ervin R. Heald of the Aircraft Division, Long Beach, in particular, for permission to present the data of Refs. 1 and 2.

* Manager, Dynamics Section, Aerodynamics and Propulsion Research Laboratory. Associate Fellow Member AIAA.

Introduction

A MAJOR influence of aeroelasticity on the flying qualities of aircraft is found in the lateral-directional characteristics. Large quantitative changes are introduced on the static directional stability, the aileron effectiveness, and the dihedral effect by vehicle flexibility. The loss of vertical tail lift effectiveness due to aeroelastic behavior is a critical problem because the vertical tail is the only source of static directional stability, whereas both the horizontal tail and the wing determine static longitudinal stability. The loss of aileron effectiveness is a critical problem because of the requirements for roll control in high-speed flight. The dihedral effect can be a critical aeroelastic problem because of the importance of dihedral in determining dynamic stability in the spiral and Dutch roll modes of motion and the large changes in dihedral that result from symmetrical wing bending during longitudinal maneuvers that approach limit load factor. The role of aeroelasticity in the estimation of directional stability and aileron effectiveness is well known, but it would appear that the potential magnitude of aeroelastically induced changes in the dihedral effect is not generally appreciated if one may judge from the lack of discussion of the topic in the stability and control literature of the past decade. The purposes of this paper are to present some recently declassified experimental data of the rolling moment caused by sideslip measured at low speed on a flexible (flutter) model of the Douglas XA3D-1 airplane, to recall some early simplified methods of analysis, and to outline how new advances in lifting surface theory can be employed for the estimation of the dihedral effect through the use of aerodynamic influence coefficients.

Experimental Results

A series of wind-tunnel tests was conducted on a $\frac{1}{12}$ scale aeroelastic model of the Douglas (El Segundo) XA3D-1 airplane in the closed, three-dimensional working section of the GALCIT (Guggenheim Aeronautical Laboratory, California Institute of Technology) 10-ft low-speed wind tunnel during August 1952. The Douglas XA3D-1 medium bomber is a high-wing monoplane with a sweptback wing and tail group and is powered by two jet engines mounted in nacelles underneath the wing. The geometrical characteristics of its wing are shown in Table 1.

The GALCIT tests were conducted to obtain basic lift and pitch data, horizontal tail and elevator effectiveness, basic yaw data, vertical tail and rudder effectiveness, and aileron and spoiler effectiveness as they are influenced by aeroelasticity. Both static and dynamic tests were run, the dynamic tests being of the single degree-of-freedom type in both pitch and yaw. The static tests were run using the basic configuration and the tail-off configuration; the dynamic tests were conducted with the basic configuration and the wing-off configuration. The tunnel dynamic pressure was varied from 10 psf up to 40 psf on the yaw runs and up to 50 psf on the longitudinal runs. The maximum Mach number and Reynolds number of these tests were about 0.20 and 1.4×10^6, respectively.

The wind-tunnel model was a $\frac{1}{12}$ scale simulation of the airplane designed to duplicate its structural and inertial properties for the design flight condition of 56,000 lb gross weight and center of gravity location at 15.2% of the mean aerodynamic chord. Single 75 ST aluminum spars located along the elastic axes of the wing, nacelle, pylon, horizontal and vertical tails were scaled to represent the elastic properties of these components. The model was constructed of balsa sections fastened to the spars. Small lead weights were distributed within each section to obtain the proper inertial properties. The inertial properties of the control surfaces were simulated but the elastic properties were not, although leaf springs were provided to represent aileron control cable elasticity, and the ailerons, elevator, and rudder could be clamped in any desired angular position. The fuselage was essentially rigid. A list of model scale factors is given in Table 2.

For the static tests a tandem vertical strut system was used with the GALCIT image system angle-of-attack mechanism linked to the tail strut to vary the angle of attack. The six-component data required for these tests were obtained by the use of a strain-gage sting balance system that was mounted inside the fuselage. The model could not be yawed during a run, and so yaw data were obtained from a series of runs, each at a given yaw angle, at two angles of attack, and for several values of the tunnel dynamic pressure. In addition to the force data, photographs were taken of small white tabs mounted on the leading and trailing edges of the wing and horizontal tail in an attempt to determine the maximum deflection of these surfaces at the various model attitudes and loading conditions. Throughout most of the tests snubbing-wires were attached to the model in order to stop any flutter that may have developed; the data were corrected for interference from the snubbing-wires. The test results have been reported in Ref. 1 and analyzed in Ref. 2.

Table 1 Full scale wing dimensional data

Area	779 ft²
Span	72.5 ft
Root chord	16.136 ft
Tip chord	5.408 ft
Mean aerodynamic chord	11.682 ft
Aspect ratio	6.75
Sweepback of quarter chord line	35.92°
Taper ratio	0.335
Geometric dihedral angle	0°
Geometric twist	0°
Incidence relative to fuselage reference line	4.00°

Table 2 Model scale factors

Length	$\frac{1}{12}$
Velocity	$\frac{1}{5}$
Atmospheric density	1
Weight	$\frac{1}{1728}$
Moment of inertia	$\frac{1}{248832}$
Force	$\frac{1}{3600}$
Stiffness (bending and torsion)	$\frac{1}{518400}$
Deflection	$\frac{1}{12}$
Twist	1

The data on wing dihedral effect were measured during run numbers 70 and 72–76 of Ref. 1, which obtained basic yaw data for the tail-off configuration at six yaw angles: $\Psi = -5°, -3°, -1°, +1°, +3°$, and $+5°$ (note $\Psi = -\beta$); at two angles of attack: $\alpha_a = -3°$ (the approximate angle of zero lift) and $+1°$; and at four values of tunnel dynamic pressure: $q = 10, 20, 30$, and 40 psf. The rolling moment in yaw measured on the tail-off configuration eliminates the influence of the vertical tail so that the combination of wing dihedral effect and wing-fuselage interference is obtained directly. The data for the lift coefficients and the rolling moment coefficients about the stability axis for the four values of the tunnel dynamic pressure are reproduced in Figs. 1–4. The experimental values of the dihedral effect found by the method of least squares from the slopes of the rolling moment vs yaw angle curves ($C_{l_\beta} = -dC_{l_s}/d\psi$) are summarized in Fig. 5. The corresponding average lift coefficients and equivalent load factors for the design flight gross weight of 56,000 lb are shown in Fig. 6 ($n = C_L qS/W$). The relative constancy of C_{l_β} at the four values of q at $\alpha_a = -3°$ is a result of the small wing lift and consequent slight amount of induced dihedral, whereas the large increase in dihedral effect with q at $\alpha_a = +1°$ follows from the increasing wing lift and induced dihedral.

Review of Previous Methods of Analysis

The correlation between experimental and estimated values of dihedral effect as shown in Fig. 5 is taken from Ref. 2. The difference between the curves for the two angles of attack at $q = 0$ is a property of the stability axis coordinate system. The method of estimation was developed in Ref. 3 and later published in Ref. 4. It is shown[4] that the aeroelastic increment in dihedral effect is proportional to gross weight, normal load factor, and the damping-in-roll coefficient based on the two assumptions that all of the airplane lift acts on the wing and that the wing deflection curve is parabolic. The approximate solution is

$$\Delta C_{l_\beta} = (4kW/b)nC_{l_p} \tag{1}$$

where k is a flexibility constant relating wing lift to wing tip deflection:

$$h_t = kL_w \tag{2a}$$

$$\cong knW \tag{2b}$$

The total dihedral effect is found by adding the aeroelastic increment to the value for the rigid vehicle†:

$$C_{l_\beta} = (C_{l_\beta})_0 + \Delta C_{l_\beta} \tag{3}$$

† An aeroelastic correction for the vertical tail should also be included in Eq. (3), but it is not our intention to discuss tail effects here.

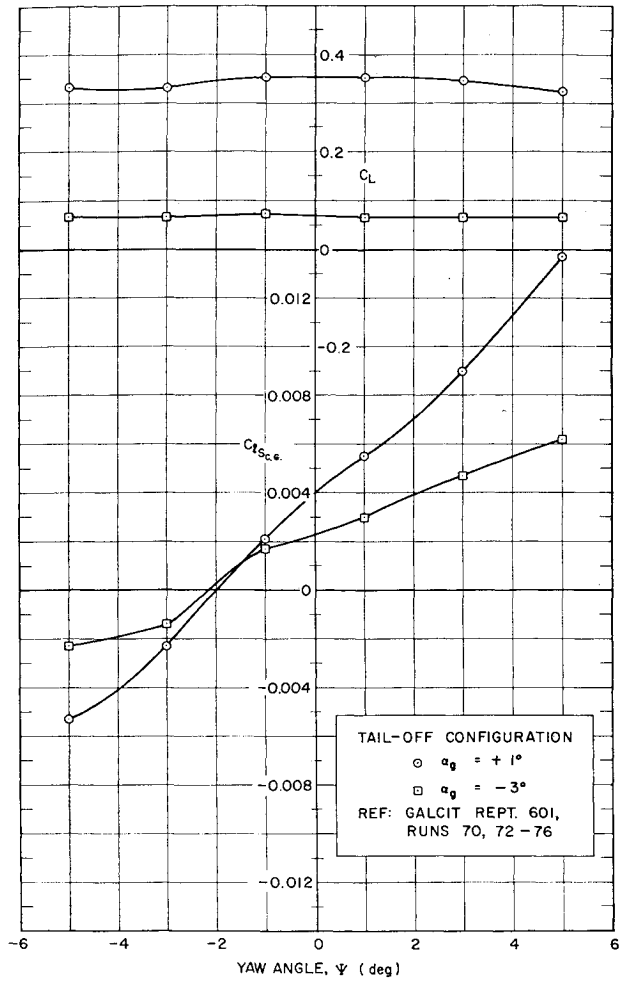

Fig. 1 Lift and rolling moment coefficients in yaw at q = 10 psf.

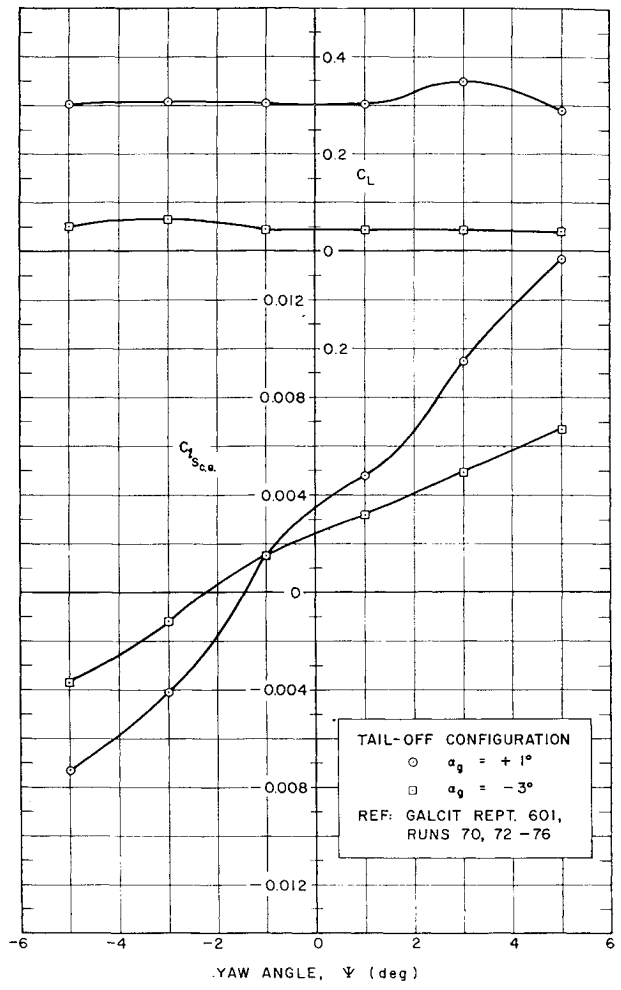

Fig. 2 Lift and rolling moment coefficients in yaw at q = 20 psf.

It was not until Ref. 4 was published that the author became familiar with an earlier NACA study by Lovell.[5] Lovell's result is more general in not restricting the wing deflection curve to a parabola, but by representing it as an mth degree curve

$$h = h_t(2y/b)^m \tag{4}$$

By utilizing the influence lines developed by Pearson and Jones,[6] which show the contribution of unit lengths of dihedral segments across the span to the rolling moment caused by sideslip in an incompressible flow, Lovell expresses the aeroelastic increment in dihedral effect as

$$\Delta C_{l_\beta} = m\left(\frac{2h_t}{b}\right)\int_0^1 \frac{d(C_{l_\beta}/\Gamma)}{d\eta}\,\eta^{m-1}d\eta \tag{5}$$

Lovell evaluated Eq. (5) graphically for a number of planform aspect and taper ratios and a range of $1 \leq m \leq 6$ and showed that the shape of the bending deflection curve is relatively unimportant in determining the aeroelastic increment in dihedral effect for $m \geq 2$, the main factor being the magnitude of wing tip deflection. Equations (1) and (5) are identical in the case $m = 2$.

The tip deflection can always be calculated if the distributions of aerodynamic lift and structural stiffness are known. For situations when such detailed information is not available, however, Lovell proposes an approximate expression based on the assumption of a uniform effective working stress σ across the span [Eq. (8) of Ref. 5]. The expression can be evaluated to read

$$h_t = 0.235(n\sigma b^2/n_L E t_r)(1 - \lambda + \lambda\log\lambda)/(1 - \lambda)^2 \tag{6}$$

With Lovell's approximations, the constant in Eq. (2) becomes

$$k = 0.235(\sigma b^2/n_L W E t_r)(1 - \lambda + \lambda\log\lambda)/(1 - \lambda)^2 \tag{7}$$

and Eq. (1) becomes

$$\Delta C_{l_\beta} = 0.94 C_{l_p}(n/n_L)(\sigma/E)(b/t_r) \times (1 - \lambda + \lambda\log\lambda)/(1 - \lambda)^2 \tag{8}$$

The magnitude of the aeroelastic increment in dihedral effect in terms of load factor may be estimated from Figs. 5 and 6 for the XA3D-1 airplane. The design limit load factor for the design flight gross weight of 56,000 lb was 2.67 and corresponds, in Fig. 6, to the tunnel dynamic pressure q = 26.5 psf at $\alpha_a = +1°$; the corresponding aeroelastic increment, from Fig. 5, is $\Delta C_{l_\beta} = -0.00102$/deg, which is 76% of the (tail-off) rigid value of C_{l_β} (−0.00135/deg). Another illustration of the magnitude of the increment is found in the two hypothetical examples given by Lovell of a fighter and a bomber. Lovell's results are reproduced‡ in Table 3. The aeroelastic increments at limit load factor for the fighter and the bomber are seen to be 58% and 92%, respectively, of the rigid values of C_{l_β}.

Analysis by Influence Coefficients

Neither Eq. (1) nor Eq. (5) is restricted to the case of incompressible flow, and each may be used in general if com-

‡ The sign of C_{l_β} has been reversed to agree with the present sign convention.

Table 3 Increment in rolling moment coefficient due to sideslip for hypothetical fighter-type and bomber-type airplanes

	Fighter	Bomber
Aspect ratio	6.0	10.0
Taper ratio	0.500	0.500
Dihedral angle, deg	5.00	4.00
Limit load factor	8.00	2.67
C_{l_β} for rigid wing	−0.0650	−0.0613
Increment C_{l_β} for load factor of 1	−0.0047	−0.0212
Increment C_{l_β} for one-half limit load factor	−0.0188	−0.0283
Increment C_{l_β} for limit load factor	−0.0376	−0.0566

pressibility corrections to C_{l_p} and $d(C_{l_\beta}/\Gamma)/d\eta$ are known. However, recent advances in lifting surface theory (surveyed in Ref. 7 for the complete range of Mach number from subsonic to hypersonic) and computer technology suggest that the estimation of dihedral effect should be reformulated in terms of structural and aerodynamic influence coefficients.

The essence of the aerodynamic lifting problem is the relationship between the distribution of lifting pressure (the pressure differential between the upper and lower surfaces) and the surface distribution of downwash velocity. The mathematical formulation of the lifting problem leads to an integral equation for the lifting pressure. The most general numerical formulation that can be made from the aerodynamic integral equation leads to a matrix of aerodynamic influence coefficients (*AICs*) that relate the control (collocation) point lifting pressures (or the control point forces, which are the local surface integrals of the pressures) to the control point downwash velocities (or the control point deflections, whose substantial derivatives are the downwash velocities). For aeroelastic analyses, *AICs* that lead to control point forces, rather than pressures, are more useful. In the problems arising from atmospheric disturbance (e.g., a gust), the *AICs* may relate the forces to the downwash directly; in the problems arising from motion of the surface (e.g., lift effectiveness, flutter), the *AICs* should relate the forces to the deflections or the streamwise slopes. We prefer the deflections to the streamwise slopes as the generalized coordinates, because the deflections have a more general meaning on a cambered surface, and deflection influence coefficients are more readily obtained from a structural analysis than slope influence coefficients. Reference 7 discusses the ingredients of matrices of *AICs* for different types of motion and for atmospheric disturbances; the various features of the quasi-static case can be shown in three equations:

$$\{F\} = (qS/\bar{c})[C_{hs}]\{h\} \tag{9a}$$

$$= (qS/\bar{c})[B][A_s][W]\{h\} \tag{9b}$$

$$= qS[B][A_s]\{w/V\} \tag{9c}$$

Equation (9a) is the defining equation for the static *AICs* $[C_{hs}]$ that relates the control point forces $\{F\}$ to the control point deflections $\{h\}$. Equation (9b) shows that the *AICs* are given by a triple product of a pressure integration matrix $[B]$, a static pressure-downwash influence coefficient matrix $[A_s]$, and a differentiation matrix $[W]$. Equation (9c) is equivalent to Eq. (9b) and offers some convenience in the present derivation.

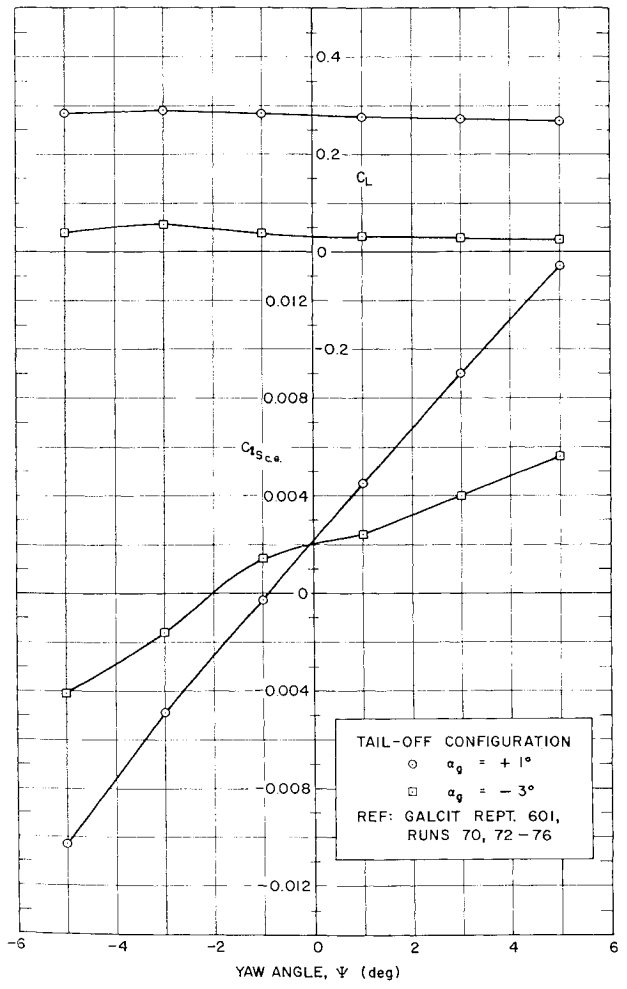

Fig. 3 Lift and rolling moment coefficients in yaw at q = 30 psf.

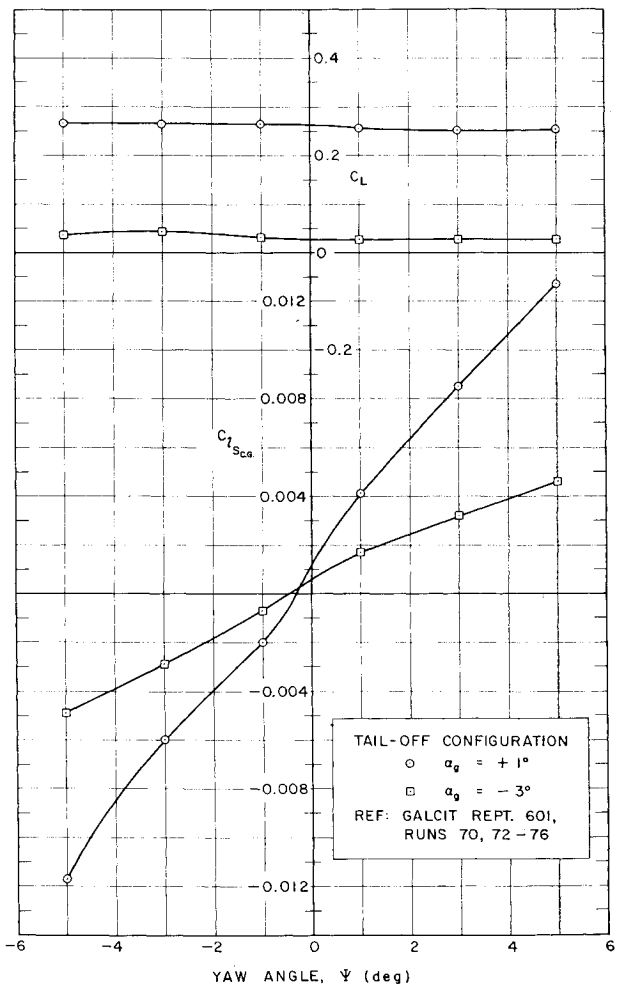

Fig. 4 Lift and rolling moment coefficients in yaw at q = 40 psf.

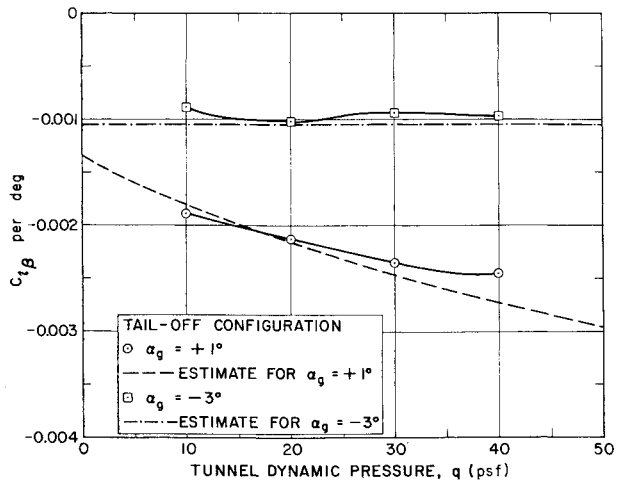

Fig. 5 Correlation of wing dihedral effect between experimental and estimated values.

Consider the loading on a symmetrical wing in sideslip. The geometry and loading are shown in Fig. 7. The spanwise coordinate is chosen positive from root to tip on both right and left wings, and it is assumed that the right and left wing control points have the same distribution with respect to the plane of symmetry. The deflections are chosen positive upward for consistency with the dihedral convention, and the control point forces are positive in the direction of the deflections. The rolling moment in sideslip may be expressed as

$$\mathcal{L} = C_{l_\beta}\beta q(2S)b \tag{10a}$$

$$= [y](\{F_l\} - \{F_r\}) \tag{10b}$$

where $[y]$ is the matrix of control point spanwise coordinates, and $\{F_l\}$ and $\{F_r\}$ are the control point forces on the left and right wing, respectively. The downwash angle on the right wing is

$$\{w/V\}_r = \{\alpha_0\} + \alpha\{I\} + \beta\{\Gamma\} + \{\partial h_r/\partial x\} + \beta\{\partial h_r/\partial y_r\} \tag{11}$$

where α_0 is the downwash angle induced by geometric twist and camber, α is the symmetrical angle of attack, β is the sideslip angle, Γ is the local initial dihedral angle, and the deflection curve slope terms can be expressed in terms of the control point deflections and matrices for differentiation in the appropriate directions:

$$\{\partial h_r/\partial x\} = [D_x]\{h_r\} \tag{12}$$

$$\{\partial h_r/\partial y_r\} = [D_y]\{h_r\} \tag{13}$$

Finally, the deflections are related to the control point forces through the structural influence coefficients assuming the fuselage to be restrained from rotation.

$$\{h_r\} = [a]\{F_r\} \tag{14}$$

Equations (9c and 11–14) may be combined and the right wing loading determined:

$$\{F_r\} = \left[[I] - (qS/\bar{c})([C_{hs}] + \beta[C_{h\beta}])[a]\right]^{-1}(\{F_s\} + \beta\{F_\beta\}) \tag{15}$$

where the *AICs* for symmetrical loading are

$$[C_{hs}] = \bar{c}[B][A_s][D_x] \tag{16}$$

the *AICs* for sideslipping are

$$[C_{h\beta}] = \bar{c}[B][A_s][D_y] \tag{17}$$

the initial (rigid) symmetrical loading is§

$$\{F_s\} = qS[B][A_s](\{\alpha_0\} + \alpha\{I\}) \tag{18}$$

and the initial (rigid) antisymmetrical loading caused by unit sideslip angle is

$$\{F_\beta\} = qS[B][A_s]\{\Gamma\} \tag{19}$$

In a similar manner we note the left wing downwash angle is

$$\{w/V\}_l = \{\alpha_0\} + \alpha\{I\} - \beta\{\Gamma\} + \{\partial h_l/\partial x\} - \beta\{\partial h_l/\partial y_l\} \tag{20}$$

where

$$\{\partial h_l/\partial x\} = [D_x]\{h_l\} \tag{21}$$

$$\{\partial h_l/\partial y_l\} = [D_y]\{h_l\} \tag{22}$$

and

$$\{h_l\} = [a]\{F_l\} \tag{23}$$

Combining Eqs. (9c and 20–23) permits determination of the left wing loading:

$$\{F_l\} = ([I] - (qS/\bar{c})([C_{hs}] - \beta[C_{h\beta}])[a])^{-1} \times (\{F_s\} - \beta\{F_\beta\}) \tag{24}$$

The difference between Eqs. (15) and (24) is required to find the rolling moment coefficient from Eq. (10). If the sideslip angle is small we may write the linearized approximation from a series expansion

$$([I] - (qS/\bar{c})([C_{hs}] \pm \beta[C_{h\beta}])[a])^{-1} \cong [I] \pm \beta(qS/\bar{c})[A]^{-1}[C_{h\beta}][a])[A]^{-1} \tag{25}$$

where

$$[A] = [I] - (qS/\bar{c})[C_{hs}][a] \tag{26}$$

by neglecting terms of order β^2. Substituting Eq. (25) into Eqs. (15) and (24) leads to the difference

$$\{F_l\} - \{F_r\} = -2\beta[A]^{-1}(\{F_\beta\} + (qS/\bar{c})[C_{h\beta}][a][A]^{-1}\{F_s\}) \tag{27}$$

from which the aeroelastic increment in wing dihedral effect

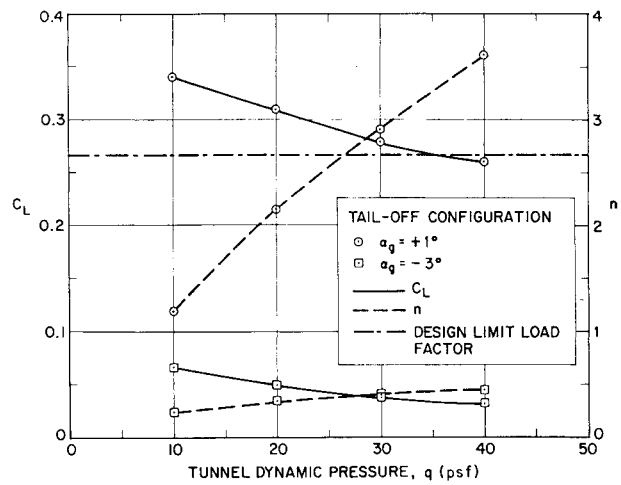

Fig. 6 Mean lift coefficient in yaw runs and equivalent load factor.

§ The symmetrical inertial loading $-ng[M]\{I\}$, where $[M]$ is the wing mass matrix, should be added to Eq. (18) for completeness. In many cases, however, it is small as compared to the aerodynamic loading, and neglecting it is consistent with the approximation that all the airplane lift acts on the wing. The term probably should be included in analyses of tailless aircraft.

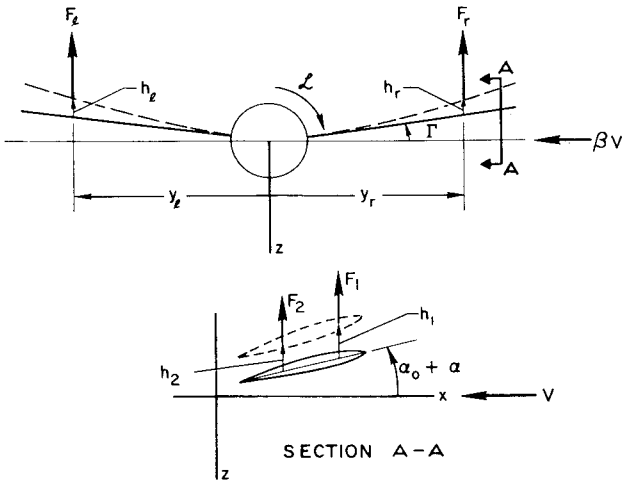

Fig. 7 Geometry and loading of sideslipping wing.

follows:

$$\Delta C_{l_\beta} = -\tfrac{1}{2}[2y/b][A]^{-1}(\{F_\beta/qS\} + (qS/\bar{c})[C_{h\beta}][a][A]^{-1}\{F_s/qS\}) \quad (28)$$

Although $\{F_s\}$ and $\{F_\beta\}$ can be estimated theoretically from Eqs. (18) and (19), respectively, they also can be obtained experimentally from pressure measurements on a rigid model; the terms $\{F_s/qS\}$ and $\{F_\beta/qS\}$ in Eq. (28) may therefore be interpreted either as theoretical or experimental force coefficients.

The first term of Eq. (28) is the aeroelastic correction to the geometric wing dihedral effect; the second term is the aeroelastic correction caused by the symmetrical load factor. The two-term expression for total dihedral effect given in Eq. (3) is therefore seen to be inadequate to account for all wing effects (as noted previously, tail effects have been excluded from this discussion) and should be expanded to read

$$C_{l_\beta} = (C_{l_\beta})_0 + (\Delta C_{l_\beta})_\Gamma + (\Delta C_{l_\beta})_n \quad (29)$$

where $(C_{l_\beta})_0$ is now interpreted as the rigid rolling moment coefficient in sideslip arising from all sources other than geometric dihedral (e.g., wing-fuselage interference, wing sweep, wing tip shape, etc.); $(\Delta C_{l_\beta})_\Gamma$ is the increment caused by the amplified geometric dihedral, and $(\Delta C_{l_\beta})_n$ is the increment caused by symmetrical wing bending and torsion. The inadequacy of Eq. (3) in no way limited the excellent correlation achieved in Fig. 5 because the XA3D-1 wing had zero geometric dihedral, and the term omitted from Eq. (29) vanishes identically in this case.

Concluding Remarks

An extensive amount of experimental data has been presented to substantiate the author's contention that the dihedral effect of a flexible wing ranks high on the list of significant aeroelastic effects on aircraft. The magnitude of the variations shown indicates, rather dramatically, the necessity of adequate estimation of the dihedral effect in order to insure accurate analysis of lateral-directional maneuvers, particularly those which are highly coupled with the longitudinal system as in the case, for example, of rolling pullouts. Correlation of the data with an early method of analysis has also been shown, and a new formulation of the problem has been presented in terms of structural and aerodynamic influence coefficients, which permits estimation of the effect in terms of data required for other aeroelastic analyses. Although no calculations were carried out by the new method on the XA3D-1 wing, it is anticipated that the correlation would be slightly improved over the simplified method.

References

[1] Ogawa, H., "Report of wind-tunnel tests on a $\frac{1}{12}$ scale aeroelastic model of the Douglas (El Segundo) XA3D-1 airplane," Guggenheim Aeronaut. Lab., Calif. Inst. Technol. Rept. 601 (April 1953).

[2] Rodden, W. P., "Analysis and summary of low-speed aeroelastic model tests of the XA3D-1 airplane," Douglas Aircraft Co., Inc., Rept. ES 17246 (February 1953).

[3] Rodden, W. P., "Static longitudinal stability and dynamic lateral stability as affected by aircraft flexibility," Douglas Aircraft Co., Inc., Rept. ES 17299 (March 1953).

[4] Rodden, W. P., "A simplified expression for the dihedral effect of a flexible wing," J. Aeronaut. Sci. **22**, 579 (1955).

[5] Lovell, P. M., Jr., "The effect of wing bending deflection on the rolling moment due to sideslip," NACA TN 1541 (February 1948).

[6] Pearson, H. A. and Jones, R. T., "Theoretical stability and control characteristics of wings with various amounts of taper and twist," NACA Rept. 635 (1938).

[7] Rodden, W. P. and Revell, J. D., "The status of unsteady aerodynamic influence coefficients," IAS Sherman M. Fairchild Fund Paper FF-33 (January 23, 1962).